Journal of Power Sources 222 (2013) 32–37

Contents lists available at SciVerse ScienceDirect

Journal of Power Sources

journal homepage: www.elsevier.com/locate/jpowsour

Short communication

Order-aligned Mn_3O_4 nanostructures as super high-rate electrodes for rechargeable lithium-ion batteries

Jiazheng Wang, Ning Du*, Hao Wu, Hui Zhang, Jingxue Yu, Deren Yang

State Key Laboratory of Silicon Materials, Department of Materials Science and Engineering, Zhejiang University, Hangzhou 310027, People's Republic of China

HIGHLIGHTS

- Mn_3O_4 layer was deposited on Cu nanowire arrays via electrochemical method.
- The 3D electrodes show improved performance as anode for Li-ion battery.
- Improved performance was attributed to the advantages of the electrodes' structure.

ARTICLE INFO

Article history:
Received 20 May 2012
Received in revised form
14 August 2012
Accepted 21 August 2012
Available online 28 August 2012

Keywords:
Manganous manganic oxide
Nanostructures
High rate
Electrodes
Lithium ion batteries

ABSTRACT

We demonstrate the synthesis of order-aligned Mn_3O_4 nanostructures by electrochemically depositing Mn_3O_4 on a pre-fabricated Cu nanowire array current collector. When used as an electrode for lithium-ion batteries, it exhibits a capacity up to 637 and 494 mA h g^{-1} after 100 cycles at a current rate of 10 C and 20 C (10 C = 9.4 A g^{-1}), respectively. The excellent cycling performance and superior rate capability can be attributed to the good electrical contact, fast electron transport and good strain accommodation of the order-aligned nanostructured electrodes. The relationship between the thickness of the Mn_3O_4 film and its electrochemical performance has also been investigated.

1. Introduction

Lithium-ion batteries are currently regarded as promising power sources for popular consumer electronics as well as upcoming electric vehicles [1–3]. Although graphite anodes are now widely used in commercial lithium-ion batteries due to high cyclability, their low capacity (372 mA h g^{-1}) can hardly meet the increasing demand for batteries with higher capacity [4]. Therefore, large research efforts have been devoted to search useful alternative materials with large capacity, high rate tolerance, and long cycle life [5–7]. Recently, transition metal oxides (Fe_2O_3, Co_3O_4, NiO, CoO) with high theoretical capacity have attracted more and more attention [8–11]. Among them, Co_3O_4 is most appealed for its high electrochemical capacity and noticeable capacity retention. Various forms of Co_3O_4 electrode materials have been tried, including Co_3O_4 nanowires, nanotubes and nanobelts [9,12,13]. However, Co based materials is confronted with its high-cost problems, which may restrict its commercial application. Compared to Co_3O_4, Mn_3O_4 exhibits a higher theoretical capacity (936 mA h g^{-1}), less toxic and more abundant in natural resources. Moreover, bulk manganese is about 20 times less expensive than cobalt [14]. Nevertheless, two serious problems greatly prohibit the application of manganese-based anode materials in high-performance lithium-ion batteries: (1) poor cyclability arising from the significant volume change during Li insertion/extraction; (2) low rate capability caused by the extremely low electrical conductivity ($\sim 10^{-7}$ to 10^{-8} S cm^{-1}) of Mn_3O_4 material [15]. To loosen the two obstacles, several strategies have been proposed such as doping Mn_3O_4 with Co, using Mn_3O_4/RGO (reduced graphene oxide) composite and nanosized Mn_3O_4 anode materials [14–16]. In most cases, these approaches can only improve the electrochemical performance of Mn_3O_4 anodes to a limited extent.

It is now recognized that an efficient way to improve the electrochemical response of active materials is optimizing electrode structures and significant improvements in battery performance were obtained by using ordered nanostructures grown directly on

* Corresponding author. Tel.: +86 571 87953190; fax: +86 571 87952322.
E-mail address: dna1122@zju.edu.cn (N. Du).

0378-7753/$ – see front matter © 2012 Elsevier B.V. All rights reserved.
http://dx.doi.org/10.1016/j.jpowsour.2012.08.056

current collector substrates as electrodes [17–20]. It has been demonstrated that this kind of electrodes allows for good electrical contact, fast electron transport and good strain accommodation [17]. Therefore, it is expected that order-aligned Mn_3O_4 nanostructured electrode could lead to an improved electrochemical performance in cyclic stability and rate capability and could be successfully used in the field of three-dimensional microbatteries.

In this paper, we report the synthesis of order-aligned Mn_3O_4 nanostructures by electrochemically depositing Mn_3O_4 on a prefabricated Cu nanowire array current collector. The as-prepared sample was directly used as electrodes of lithium-ion batteries without any ancillary materials, which afforded a high reversible capacity with good rate capability.

2. Experiment section

2.1. Synthesis of Cu nanowire arrays on a Cu substrate

Cu nano-architectured arrays were fabricated by the cathodic electrodeposition with anodized aluminum oxide (AAO) templates with the pore diameters of about 200–300 nm. Before using the cathode foil, the cathode Cu substrates were mechanically polished with 1.0 μm alpha alumina and 0.25 μm gamma alumina polishing slurry; The electrolyte systems were consisted of $CuSO_4 \cdot 5H_2O$ 100 g L^{-1}, $(NH_4)_2SO_4$ 10 g L^{-1}, diethylenetriamine (DETA) 40 g L^{-1}. The details of synthetic strategy were fully described in the previous paper [17].

2.2. Synthesis of order-aligned Mn_3O_4 nanostructures

The order-aligned Mn_3O_4 nanostructures were synthesized via an electrochemical route. The electrochemical cell consisted of a working electrode (Cu nanowire arrays), a carbon rod counter electrode, and an Ag|AgCl reference electrode. A solution with 0.1 M manganese sulfate (Aldrich) and 0.1 M sodium sulfate (Aldrich) was used as the electrolyte. The deposition of Mn_3O_4 was performed under galvanostatic conditions at a constant current of 3 mA cm^{-2} for 90 s. Four types of thickness-controlled Sn thin films were prepared for comparison by depositing for 40, 90, 180 and 300 s, respectively. After the deposition, the samples were heat-treated at 400 °C for 1 h.

2.3. Characterization and electrochemical measurement

The obtained samples were characterized by X-ray powder diffraction (XRD) with a Rigaku D/max-ga X-ray diffractometer with graphite monochromatized Cu K radiation ($\lambda = 1.54178$ Å). The morphology and structure of the obtained samples were examined by scanning electron microscopy (SEM HITACH S4800) with an energy-dispersive X-ray spectrometer (EDX) and transmission electron microscopy (TEM, PHILIPS CM200 and Tecnai G2 F20 S-TWIN, FEI). Electrochemical measurements were performed by coin type cells (CR2025) which were assembled in a glove box (Mbraun, labstar, Germany) under an argon atmosphere by directly using the final-products as the anodes. The counter and reference electrodes were lithium metal foils (15 mm diameter), and the electrolyte solution was 1 M solution of $LiPF_6$ in ethylene carbonate (EC) and dimethyl carbonate (DMC) (1:1 by volume). Finally, the cells were then aged for 12 h before measurements. A galvanostatic cycling test of the assembled cells was carried out on a Land CT2001A system in the potential range of 0.01–3.0 V at a discharge/charge current density of 936 mA g^{-1}. Cyclic voltammetry (CV) was recorded on an Arbin BT 2000 system at a scan rate of 0.1 mV s^{-1}.

The accurate mass of the active material on the Cu nanoarrays current collector was examined using a microbalance. We measured the masses of the substrate with Cu nanowire arrays and the substrate after electrodeposition, respectively. Thus, the total masses of the Mn_3O_4 film could be obtained.

3. Results and discussion

An overview of the synthetic route for order-aligned Mn_3O_4 nanostructures is shown in Fig. 1. Briefly, a typical synthetic procedure involves in two steps: 1) growth of Cu nanowire arrays on a Cu substrate via the cathodic electrochemical deposition in an AAO template; 2) deposition of a Mn_3O_4 layer onto the surface of Cu nanowires. Fig. 2a is the scanning electron microscopy (SEM) image of the Cu nanowire arrays. It can be seen that the Cu nanowires have a relatively uniform size with good alignment. After Mn_3O_4 coating for 90 s (Fig. 2b and c), the diameters of the nanowires slightly increase compared to the bare Cu nanowires, suggesting the formation of Mn_3O_4 layer. The inset magnified SEM images show that the surface of Cu nanowire turns to be rough with many Mn_3O_4 nanoflakes. Fig. 2d is the EDX spectrum of the as-synthesized product. Elements Cu, Mn and O are detected, which may come from the Cu nanoarrays current collector and Mn_3O_4 film, respectively.

The phase and purity of the samples were identified by X-ray diffraction pattern (Fig. 3). Five well-resolved peaks can be indexed to tetragonal phase of Mn_3O_4 (JCPDS card: 18-0803). In addition, the peaks at 43.3°, 50.4°, 74.1° are attributed to the Cu nanowire array current collector. No other crystalline state is observed, indicating high purity and crystallinity of the as-synthesized product. Transmission electron microscope (TEM) was employed to further investigate the morphology and structure of the product. The nanowires were scraped out of the substrate, sonicated in ethanol, and deposited on Au grids for TEM characterization. Fig. 4a and b shows typical TEM images of an individual core-shell

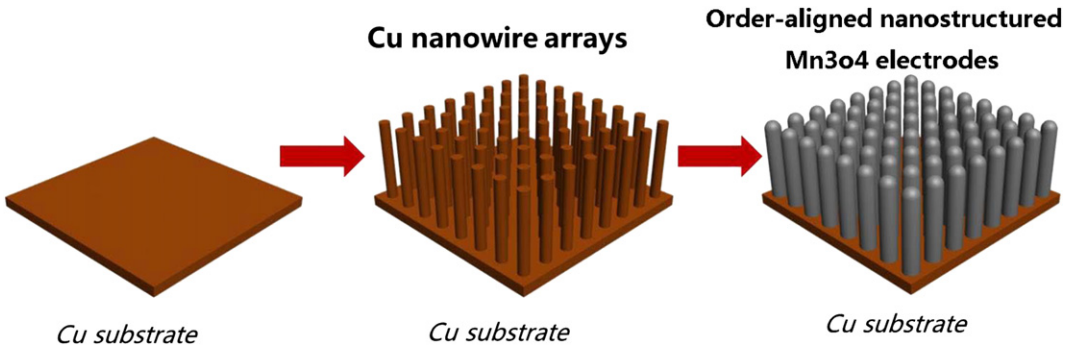

Fig. 1. (a) Schematic illustration for synthesis of the order-aligned nanostructured Mn_3O_4 electrode.

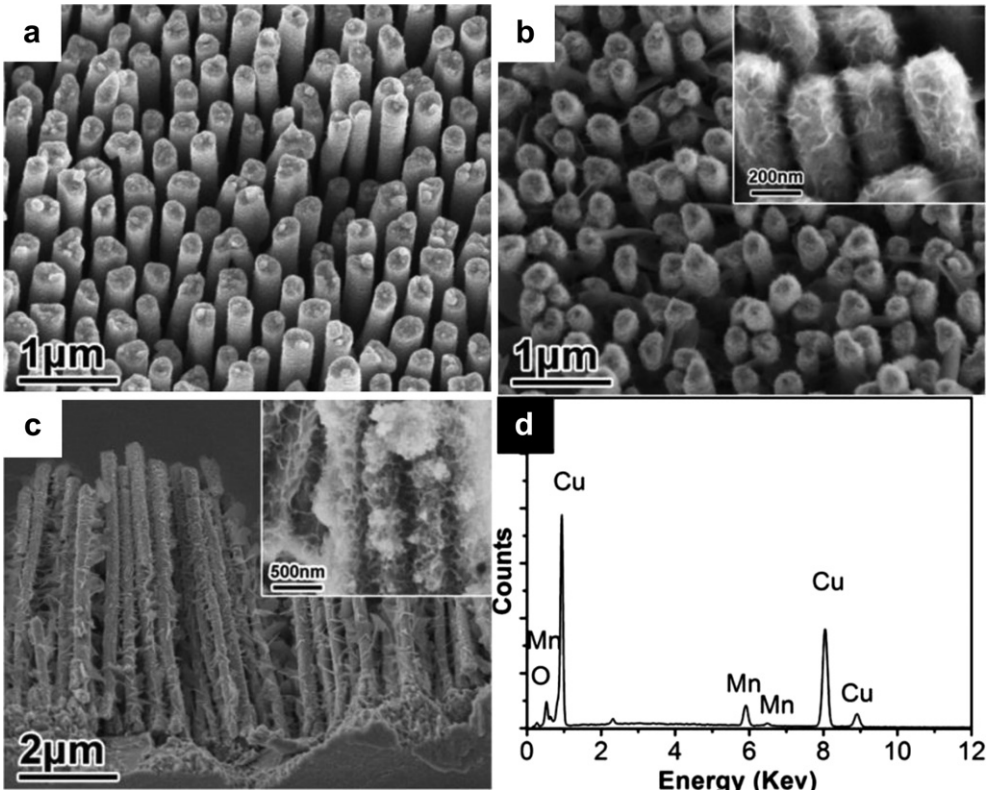

Fig. 2. (a) SEM image of the Cu nanowire arrays on a Cu substrate; (b), (c) top-view and cross-section SEM images of the order-aligned Mn_3O_4 nanostructures deposited for 90 s, the insets shows the magnified SEM images; (d) EDX spectrum of the order-aligned nanostructured Mn_3O_4 electrode.

nanostructure, in which the surface of Cu nanowire is uniformly covered with thin Mn_3O_4 nanosheets. Fig. 4c displays the images of scanning transmission electron microscopy (STEM) and EDS mapping analysis of a single nanowire, which unambiguously confirms the Cu core/Mn_3O_4 shell structure. The high-resolution TEM (HRTEM) image shown in Fig. 4d reveals the interplanar spacing of ≈0.25 nm, corresponding to the (211) plane of Mn_3O_4, which is consistent with the XRD pattern in Fig. 3.

It is generally accepted that the reaction mechanism between Li and Mn_3O_4 is a conversion reaction to form lithium oxide and metal nanoparticles, as described in equation (1):

$$Mn_3O_4 + 8Li^+ + 8e^- \leftrightarrow 3Mn(0) + 4Li_2O \quad (1)$$

In order to understand the electrochemical details of the charging/discharging process, Cyclic-voltammetric measurements were first conducted between 0.01 and 3 V. Fig. 5a shows the first three CV curves for a 90 s deposition-time electrode at a scan rate of 0.1 mV s^{-1} and a temperature of 20 °C. In the first discharge process, there was a cathodic peak located at 1.18 V which disappeared in the following cycles. This peak can mainly be ascribed to the formation of a solid electrolyte interphase (SEI) layer owing to the decomposition of electrolyte on the Mn_3O_4 film surface. The reduction peak appeared at 0.14 V was assigned to the decomposition of Mn_3O_4 into metallic Mn and Li_2O. Upon charge, one peak at around 1.23 V was observed, which was attributed to oxidation of metal Mn. In the second cycle, it is noticed that the reduction peak shifted to 0.4 V in the second cycle, which is mainly due to the drastic lithium driven, structural or textural modifications [10]. The peak intensity and integral areas of the third cycle are similar to that of the second one, suggesting high reversibility of the order-aligned nanostructured Mn_3O_4 electrode in the subsequent cycles. Fig. 5b represents the cycling performance for the above-mentioned anodes at a rate of 1 C (1 C = 936 mA g^{-1}). It can be seen that the electrode delivers an initial discharge capacity of 919 mA h g^{-1} with a first Coulombic efficiency (the ratio between charge and discharge capacities) of 67.7%. To the best of our knowledge, the Coulombic efficiency for the first cycle in this work is much higher than the previous reports on Mn_3O_4 [14–16,21]. It is interesting to note that the specific capacity gradually increase and maintain at a capacity of 882 mA h g^{-1} after 85 cycles. This phenomenon is attributed to the reversible growth of a polymeric gel-like film resulting from kinetically activated electrolyte degradation which has been well-documented in other literatures [10,11,22,23]. We then tested the performance of order-aligned nanostructures at much higher currents varied from 5 to 40 C (37.5 A g^{-1}). It can be seen from Fig. 5c that the electrodes still maintain a capacity of 833 mA h g^{-1} at 5 C after 100 cycles, showing superior cyclic stability. When the currents were further increased

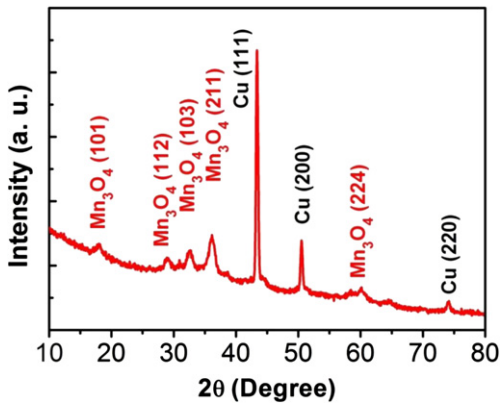

Fig. 3. XRD pattern of the order-aligned nanostructured Mn_3O_4 electrode.

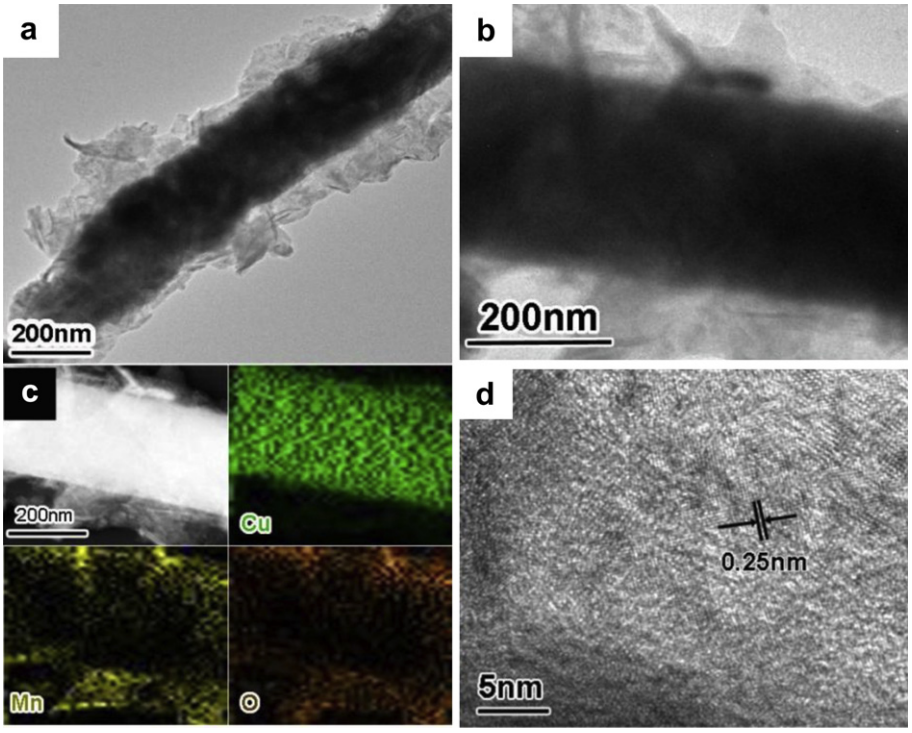

Fig. 4. (a), (b) TEM images of an individual core-shell nanostructure; (c) STEM and corresponding elemental mapping (Cu, Mn, O) of an individual Cu–Mn_3O_4 core-shell structure; (d) HRTEM of an individual Cu–Mn_3O_4 core-shell nanostructure.

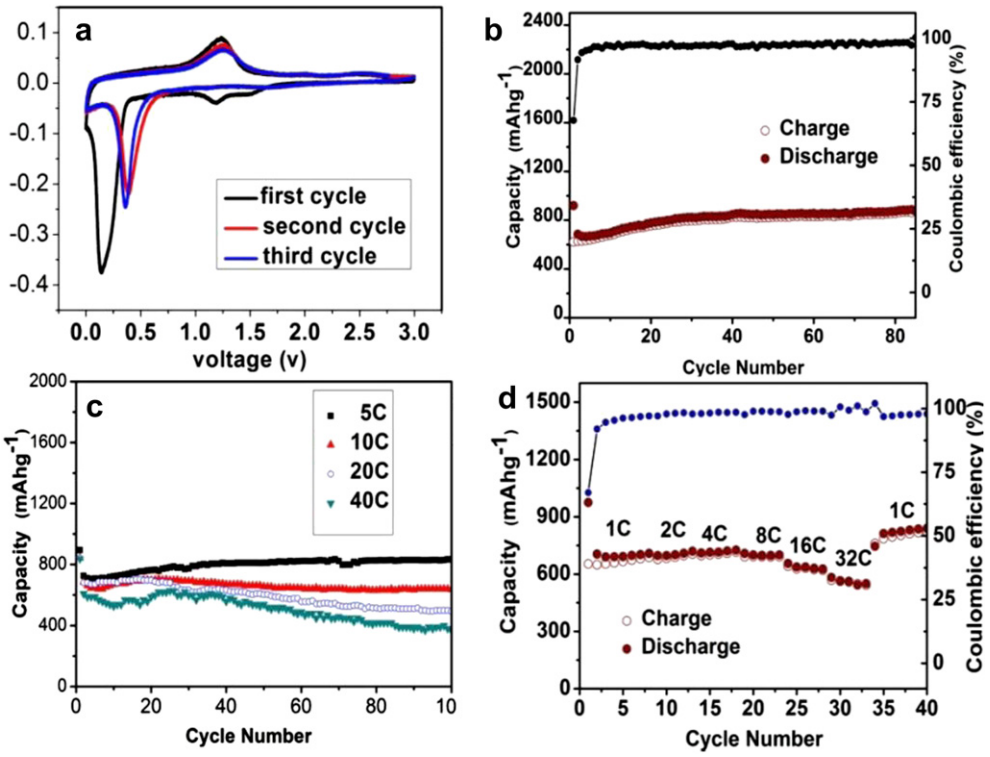

Fig. 5. (a) The first three CV curves of the order-aligned nanostructured Mn_3O_4 electrode at a scan rate of 0.1 mV s^{-1}, a temperature of 20 °C and the voltage window of 0.01–3 V; (b) discharge and charge capacities versus cycle number for the order-aligned nanostructured Mn_3O_4 electrode at the current rate of 1 C (1 C = 936 mA g^{-1}); (c) cycling performance for the order-aligned nanostructured Mn_3O_4 electrode at the current rate of 5, 10, 20 and 40 C, respectively; (d) cycling performance at various C rates of the order-aligned nanostructured Mn_3O_4 electrode.

to 10 and 20 C, the reversible capacities of 637 and 494 mA h g^{-1} could be retained, respectively. Even at a rate as high as 40 C, the electrode is capable of delivering a stable capacity of about 380 mA h g^{-1} after 100 cycles, which is still higher than the theoretical value of graphite. We could emphasis that the cycling performance at high current density of our order-aligned nanostructures surpasses all the previously published results on Mn_3O_4 [14–16,21]. Fig. 5d shows the variation of the discharge and charge capacities versus cycle numbers. As demonstrated, the electrode delivered a good fraction of its capacity and operated with a stable cycling response. For instance, it exhibits the discharge capacity of 720, 726, 700, 627, and 550 mA h g^{-1} at 2, 4, 8, 16, and 32 C (30 A g^{-1}), respectively. Once upon decreasing the rate from 32 C to 1 C, the capacity of the electrode could be restored to its original value of ~746 mA h g^{-1}, confirming the remarkable rate capability of the order-aligned Mn_3O_4 electrodes. We believe that the excellent cycling performance and superior rate capability of the order-aligned Mn_3O_4 electrode may attribute to its unique architecture: first, the order-aligned electrode has each Cu nanowire connecting with the current collector, thus led a short electron diffusion path and efficient electron transport; second, the core-shell structure ensures a large contact area between Mn_3O_4 (shell) and current collector (core), and enhanced the conductivity of the Mn_3O_4; third, the open space between neighboring of the nanowires has good accommodation of the strain, which is induced by the volume change during the electrochemical reaction; besides, the space also allows for easy diffusion of the electrolyte.

The relationship between the thickness of Mn_3O_4 film and its electrochemical performance was investigated. Fig. 6 shows the SEM pictures of the as-prepared order-aligned nanostructured Mn_3O_4 electrodes for four different deposition times ranging from 40 to 300 s. At the initial stage of the film growth, small and shapeless Mn_3O_4 nanoflakes covered the surface of the Cu nanowires as shown in Fig. 6a. Then, with the deposition time increased to 90 s, the coating layer became denser and thicker (Fig. 6b), suggesting the formation of a uniform core-shell structure. It is noted in Fig. 6c that the space among the Cu nanowires was not fully filled with Mn_3O_4 with the deposition time of less than 180 s, whereas wall-like Mn_3O_4 nanostructures covered the top of nanowire arrays when the deposition time was further prolonged to 300 s (Fig. 6d). Fig. 7 exhibits the cycling properties for the four Mn_3O_4 electrodes with different deposition time. It is indicated that the cycling performance is similar between the electrodes with the depositing time varied from 40 to 180 s. They all show excellent cycling stability, which could be explained by the above mentioned advantages of the unique order-aligned architectures. On the other hand, capacity fading was observed for the 300 s deposition-time electrode, indicating that the electrochemical performance declines when too much Mn_3O_4 material was loaded on the Cu nanowire arrays. This is mainly because there is insufficient space for efficiently buffering the volume and excess Mn_3O_4 counterbalanced the advantages of the array architecture. It is believed that the length and regularity of Cu nanowire arrays could be adjusted to make it suitable for abundant active materials.

To intuitively illustrate the advantage of order-aligned nanostructured Mn_3O_4 electrodes, we use the bare Mn_3O_4 film deposited (90 s) directly on a Cu plane substrate for comparison. It can be seen in Fig. 8a that the Mn_3O_4 layer on a planar Cu current collector shows rapid capacity decline and gives only a capacity of 361 mA h g^{-1} after 85 cycles. In a sharp contrast, the order-aligned Mn_3O_4 nanostructured electrode maintains a high reversibility, and its capacity even gradually increases to 882 mA h g^{-1}. The inset is a SEM image of the Mn_3O_4 nanostructured electrode after 20 cycles, which shows that the Mn_3O_4 layer is still stuck on the surface of the Cu nanowires and no appreciable change in the morphology could be noticed, indicating its mechanical robustness. The rate capability performances of both the samples are compared in Fig. 8b. With the increase of the current rates from 2, 4, 8,16–32 C, the measured

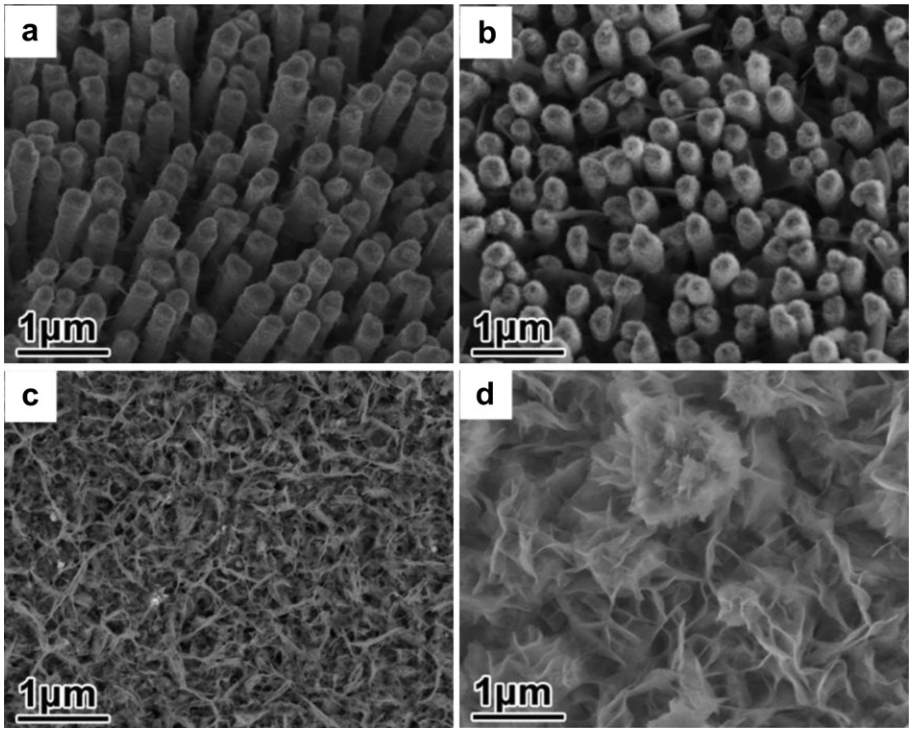

Fig. 6. SEM images of the order-aligned Mn_3O_4 nanostructures with different thickness of Mn_3O_4 layer fabricated with different deposition time: (a) 40 s; (b) 90 s, (c) 180 s and (d) 300 s, respectively.

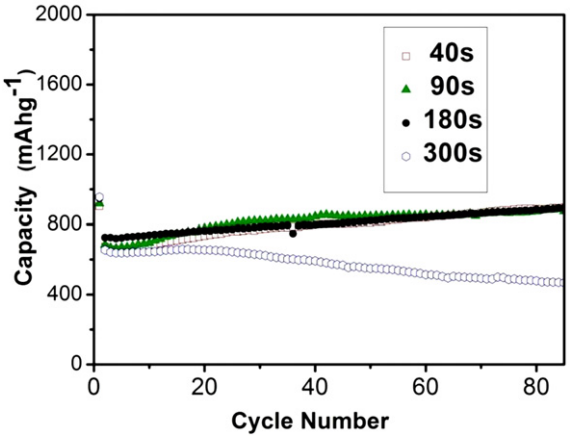

Fig. 7. Discharge capacities versus cycle number of the order-aligned nanostructured Mn_3O_4 electrode with four different thickness of Mn_3O_4 layer.

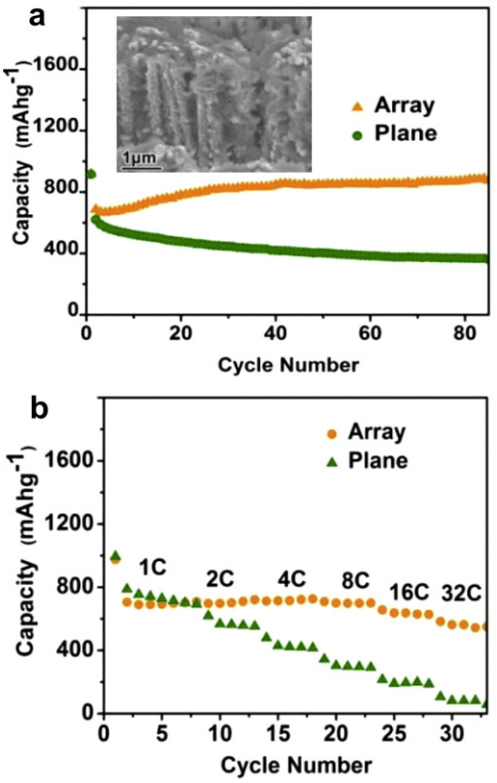

Fig. 8. (a) Cycling performance for the order-aligned nanostructured Mn_3O_4 electrode and Cu–Mn_3O_4 planer electrode at the current rate of 1 C, the inset shows cross-section view SEM image of the order-aligned nanostructured Mn_3O_4 electrode after 20 cycles; (b) cycling performance at various C rates for the order-aligned nanostructured Mn_3O_4 electrode and Cu–Mn_3O_4 planer electrode, respectively.

discharge capacities of the planar electrode are 552, 414, 290, 186 and 57 mA h g^{-1}, respectively, which is far below that of the order-aligned nanostructured electrode. This result further confirms that the order-aligned nanostructured Mn_3O_4 electrode shows the better reversible capacity and rate capability than the planar one. We believe that this nanostructured electrode can be successfully developed in the field of three-dimensional microbatteries.

4. Conclusions

In summary, order-aligned nanostructured Mn_3O_4 electrode were successfully fabricated by electrochemically depositing the Mn_3O_4 film on a pre-synthesized Cu nanowire arrays current collector. When it was directly used as the anodes for lithium-ion batteries, a high reversible capacity up to 882 mA h g^{-1} after 85 cycles at a rate of 1 C (936 mA g^{-1}) was obtained. It also exhibited a superior rate capability with a capacity up to 637 and 494 mA h g^{-1} after 100 cycles at a current of 10 C and 20 C (18.7 A g^{-1}), respectively. The improved electrochemical performance can be attributed to the efficient buffering of the volume change, fast transport of electron and good contact to the substrate of the order-aligned nanostructured electrode. We believe that the binder-free Mn_3O_4 nanostructured electrode could be a promising candidate for high rate capability, low-cost and environmentally friendly lithium-ion batteries.

Acknowledgment

The authors would like to appreciate the financial support from the 863 Project (No. 2011AA050517), NSFC (No. 51002133) and Innovation Team Project of Zhejiang Province (2009R50005).

References

[1] B. Scrosati, Nature 373 (1995) 557–558.
[2] J. Tarascon, M. Armand, Nature 414 (2001) 359–367.
[3] R. Huang, X. Fan, W. Zhu, J. Shen, Appl. Phys. Lett. 95 (2009) 133119.
[4] C. Chan, X. Zhang, Y. Cui, Nano Lett. 8 (2008) 307–309.
[5] Y. Wang, G. Cao, J. Mater. Chem. 17 (2007) 894–899.
[6] Y. Hu, L. Kienle, Y. Guo, J. Maier, Adv. Mater. 18 (2006) 1421–1426.
[7] Q. Pan, H. Wang, Y. Jiang, J. Mater. Chem. 17 (2007) 329–334.
[8] K. Brezesinski, J. Haetge, J. Wang, S. Mascotto, C. Reitz, A. Rein, S. Tolbert, J. Perlich, B. Dunn, B. Torsten, Small 7 (2011) 407–414.
[9] Y. Li, B. Tan, Y. Wu, Nano Lett. 8 (2008) 265–270.
[10] X. Wang, X. Li, X. Sun, F. Li, Q. Liu, Q. Wang, D. He, J. Mater. Chem. 21 (2011) 3571–3573.
[11] J. Do, C. Weng, J. Power Sources 146 (2005) 482–486.
[12] N. Du, H. Zhang, B. Chen, J. Wu, X. Ma, Z. Liu, Y. Zhang, D. Yang, X. Huang, J. Tu, Adv. Mater. 19 (2007) 4505–4509.
[13] L. Tian, H. Zou, J. Fu, X. Yang, Y. Wang, H. Guo, X. Fu, C. Liang, M. Wu, P. Shen, Q. Gao, Adv. Funct. Mater. 20 (2010) 617–623.
[14] J. Gao, M. Lowe, H. Abruna, Chem. Mater. 23 (2011) 3223–3227.
[15] H. Wang, L. Cui, Y. Yang, H. Casalongue, J. Robinson, Y. Liang, Y. Cui, H. Dai, J. Am. Chem. Soc. 132 (2010) 13978–13980.
[16] D. Pasero, N. Reeves, A. West, J. Power Sources 141 (2005) 156–158.
[17] P. Taberna, S. Mitra, P. Poizot, P. Simon, J. Tarascon, Nat. Mater. 5 (2006) 567–573.
[18] J. Hassoun, S. Panero, P. Simon, P. Taberna, B. Scrosati, Adv. Mater. 19 (2007) 1632–1635.
[19] J. Wang, N. Du, H. Zhang, J. Yu, D. Yang, J. Phys. Chem. C 115 (2011) 23620–23624.
[20] J. Wang, N. Du, H. Zhang, J. Yu, D. Yang, J. Mater. Chem. 22 (2012) 1511–1515.
[21] Q. Fan, M. Whittingham, Electrochem. Solid-State Lett. 10 (2007) A48–A51.
[22] S. Grugeon, S. Laruelle, L. Dupont, J. Tarascon, Solid State Sci. 5 (2003) 895–904.
[23] G. Zhou, D. Wang, F. Li, L. Zhang, N. Li, Z. Wu, L. Wen, G. Lu, H. Cheng, Chem. Mater. 22 (2010) 5306–5313.